A Techno-Economic Study of Photovoltaic-Solid Oxide Electrolysis Cells Coupled Magnesium Hydrides-based Hydrogen Storage and Transportation Toward Large-Scale Applications of Green Hydrogen

Xusheng Wang [a], Longfei Shao [a], Shouyi Hu,[a] Zi Li [a], Hangzuo Guo [c], Jiaqi Zhang [a], Yingyan Zhao,[a] Xi Lin [a], Binjian Nie [c], Zhigang Hu [, a], Jianxin Zou [*a,b]*

[a] Shanghai Key Laboratory of Hydrogen Science & Center of Hydrogen Science, School of Materials Science and Engineering, Shanghai Jiao Tong University, Shanghai, 200240, China

[b] Cambridge Graphene Center, Department of Electrical Engineering, University of Cambridge, Cambridge, CB3 0FA, United Kingdom

[c] Department of Engineering Science, University of Oxford, Oxford OX1 3PJ, United Kingdom

Contents

1 Energy analysis model of PV-SOEC- MgH_2 3

1.1 Photovoltaic cell 3

1.2 Solid oxide electrolytic cell 3

1.3 MgH_2-based hydrogen storage tank 7

1.4 Heat exchanger 11

1.5 Compressor 11

2 Exergy analysis model 12

2.1 Hydrogen production and charging 12

2.2 Hydrogen transport 14

2.3 Hydrogen supply 15

3 Exergoeconomic analysis model 16

4 Levelized cost of hydrogen (LCOH) 17

Figure S1 18

Figure S2 19

Figure S3. 20

Figure S4. 21

Figure S5 22

Figure S6 23

Figure S7. 24

Figure S8.. 25

Table S1 26

Table S2 27

Table S3. 28

Table S4 29

Table S5 30

Table S6. 31

Table S7 32

Nomenclature 33

Reference 35

1 Energy analysis model of PV-SOEC- MgH_2

1.1 Photovoltaic cell

Photovoltaic (PV) cell can directly convert solar energy into electricity, and PV arrays are composed of multiple photovoltaic cells connected in both series and parallel to generate the required power. The generally used and simplified PV model from the mono-crystalline and polycrystalline silicon PV modules is given in **Eq. S1-2** [1-2].

$$P_{PV} = N_{PV} \frac{G_I}{G_{I,ref}} \left[P_{PV,\max} + \mu_p \left(T_{PV} - T_{PV,ref} \right) \right] \tag{S1}$$

$$T_{PV} = T_a + G_I \left[\frac{NOCT - 20}{800} \right] \tag{S2}$$

Where, N_{PV} is the number of PV modules; G_I and $G_{I,ref}$ are the solar irradiance and the reference solar irradiance, respectively; W m^{-2}; $P_{PV,max}$ represents the maximum power of a single PV module, kW; μ_p stands for the power thermal coefficient, % $°C^{-1}$; T_{PV} and $T_{PV,ref}$ are the real-time photovoltaic cell temperature and the PV module temperature under standard conditions, respectively, K; T_a is the ambient temperature, K; NOCT refers to the nominal operating cell temperature, K.

1.2 Solid oxide electrolytic cell

Solid oxide electrolytic cell (SOEC) can efficiently electrolyze water and/or CO_2, and store electrical energy and thermal energy in the form of chemical energy, such as H_2, syngas (CO/H_2), etc. The required electricity for the electrolysis process is provided by the photovoltaic array, while the required heat comes from the SOEC gas recovery heat, the released heat in hydrogenation, and supplementary electrical

heating. The overall electrochemical reaction inside SOEC stacks is as follows, in **Eq. S3**:

$$H_2O \rightarrow H_2 + \frac{1}{2}O_2 \tag{S3}$$

Where, the reactions in cathode and anode are given as follow, respectively, in **Eq. S4-5**:

$$Cathode: \quad H_2O + 2e^- \rightarrow H_2 + O^{2-} \tag{S4}$$

$$Anode \quad 2O^{2-} \rightarrow O_2 + 2e^- \tag{S5}$$

The built SOEC model aims to reflect the mass and heat transfer, as well as the electrochemical reactions inside the electrolytic cells. The required electrical energy for SOEC involves the open circuit potential and the overpotential [3], the open circuit potential can be obtained by the Nernst equation. However, the actual potential of SOEC is always higher than the Nernst potential, as given in **Eq. S6-7**.

$$E^{OCP} = E_0 + \frac{RT}{2F}\ln\left(\frac{P_{H_2}P_{O_2}^{1/2}}{P_{H_2O}}\right) \tag{S6}$$

$$U = E^{OCP} + \eta_{\text{act}} + \eta_{ohm} + \eta_{con} \tag{S7}$$

Where, E^{OPC} is the open circuit potential, V; E^0 is the reversible cell voltage, V; R is the universal gas constant, J mol^{-1} K^{-1}; T is the cell temperature, K; F is the Faraday's constant, C mol^{-1}; P is the partial pressure of species, bar; η_{act}, η_{ohm} and η_{con} are the activation overpotential, the ohmic overpotential and the concentration overpotential, respectively, V.

The activation overpotential consists of the anode activation overpotential and the cathode activation overpotential, which is caused by the chemical kinetics of the electrochemical reactions, and directly determined by the electrochemical reaction

rates and the operation conditions of SOEC, as given in **Eq. S8-9** [4].

$$\eta_{\mathrm{act},i} = \frac{RT}{F}\ln\left[\frac{J}{2J_{o,i}} + \sqrt{\left(\frac{J}{2J_{0,i}}\right)^2 + 1}\right] \tag{S8}$$

$$J_{0,i} = r_i \exp\left(-\frac{E_{act,i}}{RT}\right) \tag{S9}$$

Where, J is the current density, A m^{-2}; J_0 is the exchange current density at the electrode, A m^{-2}; r is the pre-exponential factor, A m^{-2}; E_{act} is the activation energy, kJ mol^{-1}; the subscript "i" represents the cathode (i=c) and anode (i=a) of the electrolytic cells.

The ohmic overpotential is directly determined by the ionic conductivity and thickness of the electrolyte, can be given in **Eq. S10-11** [5].

$$\eta_{\mathrm{ohm}} = JL\phi \tag{S10}$$

$$\phi = 2.99\times10^{-5}\exp\left(\frac{10300}{T}\right) \tag{S11}$$

Where, L is the thickness of the electrolyte, m; J is the current density inside electrolytic cell stacks, A m^{-2}; ϕ is the resistance of the electrolyte, Ω m^{-1}.

The concentration overpotential is caused by the mass transfer resistance between the electrode and electrolyte, which reflects the difference between electrochemical reaction rates and the species diffuse rates, given in **Eq. S12-13** [6].

$$\eta_{\mathrm{con,c}} = \frac{RT}{2F}\ln\left[\frac{\left(P_{H_2} + JRTd_c / 2FD^{eff}_{H_2O}\right)P_{H_2O}}{\left(P_{H_2O} - JRTd_c / 2FD^{eff}_{H_2O}\right)P_{H_2}}\right] \tag{S12}$$

$$\eta_{\mathrm{con,a}} = \frac{RT}{4F}\ln\left[\frac{\sqrt{\left(P_{O_2}\right)^2 + \left(JRT\mu d_a / 2FB_g\right)}}{P_{O_2}}\right] \tag{S13}$$

Where, d is the thickness of the electrode, m; D^{eff}_{H2O} is the effective diffusion coefficient of the steam, $m^2\ s^{-1}$; μ is the dynamic viscosity of the oxygen, Pa s.

In this work, the Fick's model is used to calculate the diffusion coefficient at the electrode, which is given in **Eq. S14** [7].

$$\frac{1}{D^{eff}_{H_2O}} = \frac{\xi}{n}\left(\frac{1}{D_{H_2-H_2O}} + \frac{1}{D_{H_2O,k}}\right) \tag{S14}$$

Where, ξ is the electrode tortuosity; n is the electrode porosity; $D_{H2\text{-}H2O}$ and $D_{H2O,k}$ are the Knudsen diffusion coefficient and the molecular diffusion coefficient, respectively, which can be given as **Eq. S15-16** [8].

$$D_{H_2O,k} = \frac{4}{3} r \sqrt{\frac{8RT}{\pi M_{H_2O}}} \tag{S15}$$

$$D_{H_2-H_2O} = 0.00133\left(\frac{1}{M_{H_2}} + \frac{1}{M_{H_2O}}\right)^{1/2} \frac{T^{3/2}}{P\sigma^2_{H_2,H_2O}\Omega_D} \tag{S16}$$

Where, M_{H2O} and M_{H2} are the molar weights of steam and hydrogen, respectively, g mol^{-1}; r is the mean pore radius, m; $\sigma_{H2\text{-}H2O}$ is the mean characteristics length of species, such as H_2O and H_2, m; Ω_D is the dimensionless diffusion collision integral.

In **Eq. S13**, Bg is the flow permeability, given in **Eq. S17** [8].

$$B_g = \frac{n^3}{72\xi(1-n)^2}(2r)^2 \tag{S17}$$

Besides the electrochemical model, a complete SOEC model also involves the mass and heat balance equations. The current density and the reacted steam in electrolytic cells are given as **Eq. S18-19,** respectively.

$$J = \frac{n_e U_f F N_{H_2O}}{N_{cell}} \tag{S18}$$

$$N_{H_2,product} = \frac{J}{2F} \tag{S19}$$

Where, n_e is the amount of electrons; U_f is the steam utilization factor; N_{H2O} is the molar flow rate of feed water, mol s^{-1}; N_{cell} is the number of electrolytic cells.

The energy balance equation inside electrolytic cell stacks can be reflected by **Eq. S20**.

$$\sum E_{i,in} + P_{ele} - \sum E_{i,out} - N_{H_2,prouct}\Delta H = 0 \tag{S20}$$

Where, E_{in} represents the energy carried by the input species, kJ; E_{out} is the energy carried by the output species (hydrogen, steam, oxygen, air), kJ; P_{ele} is the consumed power in the electrolysis process, kW; ΔH is the reaction enthalpy in the electrolysis process, kJ.

Based on the mass, energy, and electrochemical models of SOEC, the efficiency of electrolytic cells is given in **Eq. S21**.

$$\eta_{SOEC} = \frac{N_{H_2,product} \cdot LHV_{H_2}}{UJA_{cell}N_{cell} + Q_{consumed}} \tag{S21}$$

Where, the LHV_{H2} represents the lower heat value of hydrogen, kJ mol^{-1}, A_{cell} is the active area of the single electrolytic cell, m^2; $Q_{consumed}$ is the consumed heat energy in the process of both evaporating water and raising fluids temperature, kJ.

1.3 MgH_2-based hydrogen storage tank

In the process of hydrogenation, hydrogen molecules diffuse to the metal surface and physically get adsorbed onto the surface of magnesium via van der Waals forces [9]. Then, the H_2 molecules dissociate into individual hydrogen atoms and chemically adsorb into the magnesium by diffusion to subsurface lattice sites, the reaction formula of this hydrogenation process is given in **Eq. S22** [10]:

$$Mg + H_2 \rightarrow MgH_2 \quad \text{(S22)}$$

A two-dimensional radial model is built in this work by the finite volume technique implemented COMSOL Multiphysics to simulation the magnesium hydrogenation processes, the geometric structure is given as **Figure S1**. A single hydrogen storage tank is made of 316L stainless steel with a length of 2m. The diameters of the hydrogen storage tank, thermal oil tube, and hydrogen inflow channel are 300mm, 30mm and 60mm, respectively.

1) Thermodynamic and kinetic parameters in magnesium hydrogenation processes

The equilibrium pressure in the absorption and desorption hydrogen can be given as **Eq. S23** according to the van't Hoff equation, which is defined by the temperature and concentration of the magnesium hydrides [11].

$$P_{\text{eq}} = f\left(\frac{H}{M}\right)\exp\left[-\frac{\Delta H}{R}\left(\frac{1}{T}-\frac{1}{T_{ref}}\right)\right] \quad \text{(S23)}$$

Where, *f(H/M)* is the PCT (Pressure-Composition-Temperature) curve of the solid-state hydrogen storage materials at a reference temperature of T_{ref} [12]; H/M is the hydrogen to metal ratio per metal atom; ΔH is the reaction enthalpy, equals to 75 kJ mol^{-1} and 75.5 kJ mol^{-1} for hydrogen absorption and desorption reactions, respectively.

The kinetics rate laws in magnesium hydrogenation are quite complex due to several mechanisms simultaneously occurring at subsurface lattice sites. According to the Arrhenius law, the relationships between temperature and reaction rate can be given in **Eq. S24**:

$$k\left(T,P\right)=k_0\cdot f\left(P\right)\cdot e^{-\frac{E_a}{RT}} \tag{S24}$$

Where, E_a is the activation energy, kJ mol^{-1}; *f(P)* is the pressure item.

Fitting based on the experimental results conducted by Chaise et al [12], the kinetic rate laws for hydrogen absorption can be given in **Eq. S25**.

$$\frac{d\alpha}{dt}=\begin{cases} k\cdot e^{-E_a/RT}\cdot(\frac{P-P_{eq}}{P_{eq}})\cdot\frac{\alpha-1}{2\cdot\ln(1-\alpha)}, & (P>2P_{eq}) \\ k\cdot e^{-E_a/RT}\cdot(\frac{P-P_{eq}}{P_{eq}})\cdot(1-\alpha), & (P>2P_{eq}) \\ -2\cdot k\cdot e^{-E_a/RT}\cdot\ln(\frac{P_{eq}}{P})\cdot\alpha\cdot(-\ln\alpha)^{1/2}, & (P>2P_{eq}) \end{cases} \tag{S25}$$

Where, k is the coefficient independent of pressure, α is the reaction fraction.

2) <u>Heat transfer equations</u>

The heat transfer process in a metal hydride bed mainly consists of heat conduction in the metal hydride bed and the hydrogen gas, the heat convection between the hydrogen gas and the metal materials, the chemical reaction heat, and the heat convection between the metal hydride bed and the thermal oil, is described as **Eq. S26**.

$$d_Z\left(\rho C_p\right)_{eff}\frac{\partial T}{\partial t}+d_Z\rho_g C_{p,g}u_g\cdot\nabla T=d_Z k_{eff}\cdot\nabla T+q_0+Q \tag{S26}$$

Where, d_Z is the length of the hydrogen storage tank, m; $(\rho C_p)_{eff}$ is the effective heat capacity, J K^{-1}; λ_{eff} is the effective thermal conductivity, W m^{-1} K^{-1}; ρ_g, $C_{p,g}$ and u_g are the density, specific heat capacity, and flow rate of the hydrogen, respectively; Q is the chemical reaction heat, kJ; q_0 is the heat flux between the metal hydride and the thermal oil, W m^{-2}.

The effective heat capacity and thermal conductivity of the metal hydride bed can be given in **Eq. S27-28**:

$$(\rho C_p)_{eff} = \varepsilon \rho_g C_{p,g} + (1-\varepsilon)\rho_s C_{p,s} \quad \text{(S27)}$$

$$\lambda_{eff} = \varepsilon \lambda_g + (1-\varepsilon)\lambda_s \quad \text{(S28)}$$

Where, the subscribe "*s*" and "*g*" represent solid materials and hydrogen gas, respectively; ε is the porosity of the solid-state hydrogen storage materials.

The chemical reaction heat, and the heat flux between the metal hydride and the thermal oil are given as **Eq. S29** and **Eq. S30**, respectively.

$$Q = \frac{m}{M_{\mathrm{H_2}}} \times \Delta H = \frac{\rho_s \times wt \times (1-\varepsilon)}{M_{H_2}} \times \frac{d\alpha}{dt} \times \Delta H \quad \text{(S29)}$$

$$q_0 = h\left(T - T_{oil}\right) \quad \text{(S30)}$$

Where, T_{oil} is the temperature of thermal oil, K; M_{H2} is the molar mass of hydrogen, g mol^{-1}; m is the absorbed or desorbed hydrogen molar flow rate, mol s^{-1}.

3) Mass transfer equations

The mass balances in the diffusion process in a metal hydride bed can be described by Darcy's equation, and is given in **Eq. S31**:

$$\frac{\partial}{\partial t}\left(\varepsilon_p \rho\right) + \nabla \cdot \left(\rho_g \cdot -\frac{\kappa}{\mu}\nabla \rho\right) = Q_m \quad \text{(S31)}$$

Where, κ and μ are the permeability (m^2) and dynamic viscosity (Pa s), respectively; Q_m is the mass source in the process of hydrogen sorption (kg m^{-3} s^{-1}), can be given in **Eq. S32**:

$$Q_m = \rho_s \times wt \times (1-\varepsilon) \times \frac{d\alpha}{dt} \quad \text{(S32)}$$

Where, *wt* is the theoretical hydrogen storage density.

4) Initial and boundary conditions

During the simulation process, the temperature, pressure, reaction fraction and

hydrogen flow rate in the initial state must be specified, given as follow:

$$T_{(t=0)} = T_0,\ P_{(t=0)} = P_0,\ \alpha_{(t=0)} = \alpha_0,\ \vec{u}_{g(t=0)} = 0 \tag{S33}$$

The boundary conditions are defined as:

$$T_g = T_{in},\ P_g = P_{in},\ u_g = u_{in}, u_{oil} = u_{oil,in} \tag{S34}$$

1.4 Heat exchanger

Heat transfer occurs in the heat exchanger, simultaneously changing the temperature of the working fluids. The output temperature of working fluids can be obtained by ε-NTU methods [13-14], given in **Eq. S35**:

$$\varepsilon = \frac{C_{heat}\left(T_{heat,in} - T_{heat,out}\right)}{C_{\min}\left(T_{heat,in} - T_{cool,in}\right)} = \frac{C_{cool}\left(T_{cool,out} - T_{cool,in}\right)}{C_{\min}\left(T_{heat,in} - T_{cool,in}\right)} \tag{S35}$$

Where, C is the heat capacity rate, J K^{-1}; the subscript "*heat*" and "*cool*" represent the heat fluid and cool fluid, respectively; C_{min} refers to the minimum value between C_{heat} and C_{cool}; T represents the temperature, K;

1.5 Compressor

In the actual process, the work condition of air compressor is a typical unsteady state process. However, it can be considered as a series of steady flow compressions for simplification. The compression process can be considered as an isentropic process, the output temperature, the consumed power, and the isentropic efficiency of compressor can be given in **Eq. S36-38** [15-16]:

$$T_{c,out} = T_{c,in}\pi_c^{(\kappa-1)/\kappa} \tag{S36}$$

$$\eta_c = \frac{T_{c,out}^s - T_{c,in}}{T_{c,out} - T_{c,in}} \tag{S37}$$

$$W_c = m_c\left(h_{c,out} - h_{c,in}\right) \tag{S38}$$

Where, $T_{c,out}$ is the actual output temperature of compressor, K; $T_{sc,out}$ is the isentropic temperature of compressor outlet, K; $T_{c,in}$ in the compressor inlet temperature, K; m_c is the compressor mass flow rate, kg s^{-1}; W_c is the compressor consumed power, kW; $h_{c,out}$ and $h_{c,in}$ are the specific enthalpy (kJ kg^{-1}) of working fluid at the compressor inlet and outlet, respectively.

2 Exergy analysis model

2.1 Hydrogen production and charging

The exergy involves physical, chemical, kinetic, and potential energy for working fluids, and the exergy analysis identifies the types, magnitudes, and locations of irreversibility in a thermodynamic system [17]. The physical exergy is defined based on the standard atmospheric conditions, given in **Eq. S39.** The chemical exergy is defined as the maximum work possibly obtained by chemical reactions at the standard atmospheric conditions, given in **Eq. S40.** And the kinetic and potential exergy are generally ignored in exergy analysis due to their negligible changes in elevation and speed [18].

$$Ex_{Ph} = m\left[\left(h-h_0\right)-T_0\left(s-s_0\right)\right] \tag{S39}$$

$$Ex_{Ch} = \sum_i y_i Ex_i^0 + RT\sum_i y_i \ln y_i \tag{S40}$$

$$Ex = Ex_{Ph} + Ex_{Ch} \tag{S41}$$

Where, Ex is the exergy value of the stream, kJ; m is the mass flow rate, kg s^{-1}; h and s are the specific enthalpy (kJ kg^{-1}) and specific entropy (kJ kg^{-1} K^{-1}), respectively; y_i refers to the molar fraction of the species; Ex^0 is the standard chemical exergy, kJ;

the subscript "0" represents the standard atmospheric conditions at 1 bar and 298.15 K.

The exergy balance to a given component can be defined by **Eq. S42**, which reflects the relationship among exergy destruction (E_{xD}), exergy fuel (E_{xF}), and exergy product (E_{xP}).

$$Ex_F = Ex_P + Ex_D \tag{S42}$$

For photovoltaic cells, the exergy analysis method is slightly different from other thermodynamics components. The energy of a PV cell involves electrical energy and thermal energy, the thermal energy is dissipated to the surroundings and is regarded as the useless energy in the electricity generation process. The exergy balance equation in a PV array is given in **Eq. S43** [19].

$$Ex_{in} = Ex_{out,use} + Ex_{loss} + Ex_D \tag{S43}$$

Where, Ex_{in}, $Ex_{out,use}$, Ex_{loss} and Ex_D are the exergy input, net useless exergy output, exergy loss and exergy destruction of PV panels.

The Ex_{in}, $Ex_{out,use}$, and Ex_{loss} can be given in **Eq. S44-46**:

$$Ex_{in} = G_I A_{PV}\left[1-\frac{4}{3}\left(\frac{T_a}{T_{sun}}\right)+\frac{1}{3}\left(\frac{T_a}{T_{sun}}\right)^4\right] \tag{S44}$$

$$Ex_{out,use} = V_m I_m \tag{S45}$$

$$Ex_{loss} = Q_{loss}\left(1-\frac{T_a}{T_{PV}}\right) \tag{S46}$$

Where, A_{PV} is the PV panel area, m^2; T_{sun} is the sun temperature, K; V_m and I_m are the maximum voltage (V) and maximum current (A) of the PV panels, respectively; Q_{loss} is the heat loss of PV, kJ, which can be obtained by **Eq. S47**.

$$Q_{loss} = h_c A_{PV}\left(T_{PV} - T_a\right) \tag{S47}$$

Where, h_c is the convective heat transfer coefficient (W m^{-2} K^{-1}) between PV panels and the ambient.

Table S3 summarizes the exergy balance equations for different components in the PV-SOEC-MgH_2 system based on the above exergy analysis approach.

2.2 Hydrogen transport

At present, there are no large-scale applications of clean transportation modes (fueled by hydrogen, ammonia, methanol, etc.) in the market. For large-scale applications, diesel-fueled trucks are primarily utilized for short-distance transportation, whereas conventional trains and ships are mainly used for long-distance transportation.

For ships and trucks, the exergy value of the consumed fuel can be calculated by **Eq. S48**.

$$Ex_{fuel} = \varepsilon_{fuel} m_{fuel} LHV_{fuel} \tag{S48}$$

Where, m_{fuel} represents the consumed fuel in transportation process, kg; LHV_{fuel} is the heat value of the fuel, kJ kg^{-1}; ε_{fuel} refers to the chemical energy factor for fuel, which can be given in **Eq. S49** [20].

$$\varepsilon_{fuel} = 1.0401 + 0.178\frac{H}{C} + 0.0432\frac{O}{C} + 0.2169\frac{\alpha}{C}[1 - 2.0628\frac{H}{C}] \tag{S49}$$

Where, C,H,O,α represent the respective mass ratios for hydrogen, oxygen, carbon and sulphur in the fuel, respectively.

For trains (electric-driven), the exergy value of consumed electricity can be calculated by **Eq. S50**.

$$Ex_{train} = P_{train} \tag{S50}$$

Where, P_{train} is the consumed electricity by trains.

2.3 Hydrogen supply

When the MgH_2 arrives at the hydrogen utilization sites, it needs to undergo the dehydrogenation and compression processes before it can be delivered to the end-user. For hydrogen used in transportation, electrical heating is usually used for dehydrogenation to release hydrogen. For hydrogen used in industry, such as gas turbine and steel making, the heat carried by high-temperature steam or gas recovered from the plant is utilized to heat the magnesium hydrides to release hydrogen. The exergy balance equations in hydrogen release and supply processes are given in **Eq. S51-53.**

$$Ex_{end-user} = Ex_{de} + Ex_{ele,co} \quad \text{(S51)}$$

$$Ex_{de} = Ex_{ele,de} + Ex_{heat} \quad \text{(S52)}$$

$$Ex_{ele,co} = P_{ele,co} \quad \text{(S53)}$$

Where, $Ex_{end\text{-}user}$ represents the exergy value of consumed energy in hydrogen release and supply processes, Ex_{de} and $Ex_{ele,co}$ are the exergy value of consumed energy in the dehydrogenation and compression processes, respectively. Ex_{heat} and $Ex_{ele,de}$ are the exergy value of consumed heat and electricity in dehydrogenation processes, respectively. $P_{ele,co}$ refers to the consumed electricity in compression processes. In the dehydrogenation processes, the compression approach is slightly different according to the requirement of application scenarios, the number of compression stages (N) and the consumed power ($P_{H2,co}$) corresponding to the specified hydrogen pressure are listed in **Table S4**.

3 Exergoeconomic analysis model

Economy and effectiveness are two important factors in evaluating energy systems, and the exergoeconomic analysis is widely used in energy system research because it combines both exergy and economic analysis to determine the overall exergy costs [21]. To calculate the final cost rate of products by defining the cost rate of system streams, the exergoeconomic balance for the k_{th} component is given in **Eq. S54** [22].

$$\sum \bar{C}_{out,k} + \bar{C}_{w,k} = \sum \bar{C}_{in,k} + \bar{C}_{Q,k} + \bar{Z}_k \tag{S54}$$

Where, $\bar{C}_{in,k}$ and $\bar{C}_{out,k}$ represent the cost rate ($ h^{-1}) of input and output stream for the k_{th} component, respectively; $\bar{C}_{w,k}$ and $\bar{C}_{Q,k}$ are the cost rate of generated power and the received heat by the k_{th} component, respectively; $\bar{Z}_k$ refers to the cost rate of the k_{th} component regarding capital investment and maintenance.

The capital cost of the component can be defined in **Eq. S55**:

$$\bar{Z} = \frac{Z_k CRF \phi}{\tau} \tag{S55}$$

Where, Z_k is the capital cost of the k_{th} component; ϕ is the maintenance factor; τ is the operating hours of the plant in one year; *CRF* is the capital recovery factor, which is given in **Eq. S56**.

$$CRF = \frac{i(1+i)^n}{(1+i)^n - 1} \tag{S56}$$

Where, n and i are the service year and the interest rate of the system, respectively. The capital cost of the main components in hydrogen production and storage processes is summarized in **Table S6**.

4 Levelized cost of hydrogen (LCOH)

The levelized cost of hydrogen (LCOH) is a fundamental evaluation approach used in the preliminary assessment of a hydrogen route, which is defined by calculating the cost of hydrogen, including the hydrogen production costs, manufacturing costs, transportation costs, storage costs, distribution costs, and other associated costs [23]. The LCOH considers the entire life cycle process of hydrogen from production to transportation, to delivery, and to the end-user utilization, defined in **Eq. S57- 58**.

$$LCOH = \frac{C_{pro} + C_{cha} + C_{S\&T} + C_{de} + C_{End-user}}{Q_{H_2}} \quad \text{(S57)}$$

$$C_{pro} = C_{CAP,pro} \times CRF + C_{O\&M,pro} + C_{UT,pro}$$
$$C_{cha} = C_{CAP,cha} \times CRF + C_{O\&M,cha} + C_{UT,cha}$$
$$C_{S\&T} = C_{storage} \times CRF + C_{O\&M,storage} + \sum_{i=2}^{i} C_{transporatation,i} \quad (i = 1, road; i = 2, rail/ship) \quad \text{(S58)}$$
$$C_{de} = C_{CAP,de} \times CRF + C_{O\&M,de} + \sum_{i=2}^{i} C_{de,i} \quad (i = 1, electrical; i = 2, heat)$$
$$C_{end-user} = C_{CAP,end-user} \times CRF + C_{O\&M,end-use} + C_{UT,end-use}$$

Where, C_{pro}, C_{cha}, $C_{S\&T}$, C_{de}, and $C_{End\text{-}user}$ represent the hydrogen production cost, charging cost, storage and transportation cost, dehydrogenation cost and the compression cost at the end-user side, respectively, \$, Q_{H2} is the hydrogen supply, kg. The calculation of the levelized cost of hydrogen in this study ranges from hydrogen production to the supply of hydrogen, and to end-user hydrogen utilization sites.

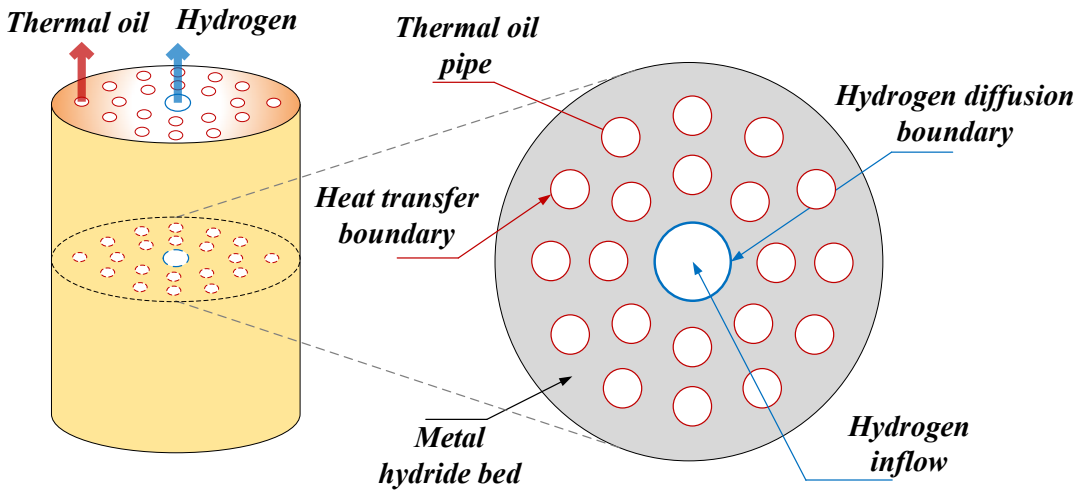

Figure S1. A geometric structure scheme of the magnesium hydrides-based hydrogen storage tank.

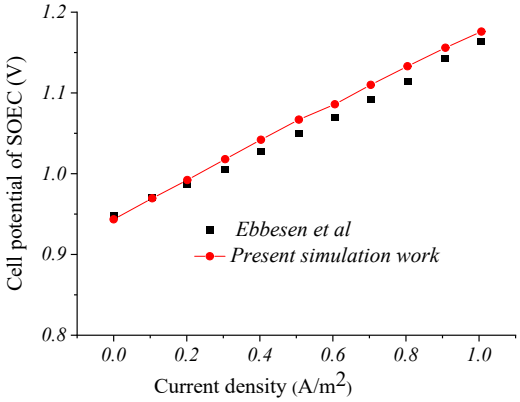

Figure S2. Validation of SOEC model [24].

Figure S3. The world's leading ton-scale Mg-based solid-state hydrogen storage and transportation trailer.

Figure S4. ***a*** Production line for magnesium-based solid-state hydrogen storage with an annual capacity of 100 tons; ***b*** Magnesium-based solid-state hydrogen storage pellets.

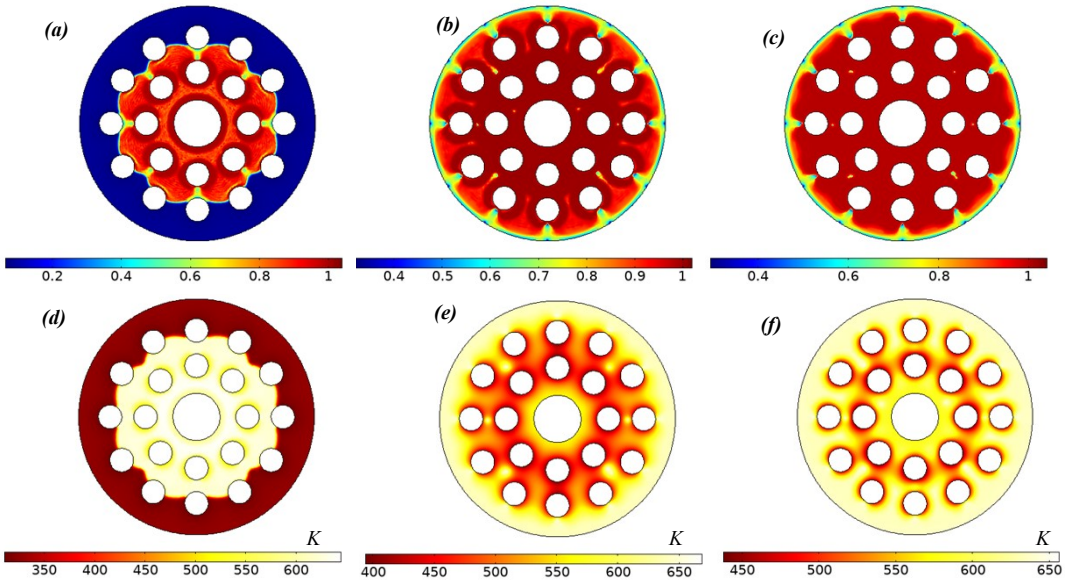

Figure S5. The reaction fraction and temperature distribution over time on the cross-section of the MH tank at $P_{gas,in}$ and $T_{gas,in}$ are 1 MPa and 573 K, respectively. ***a, b,*** and ***c*** are the reaction fraction distribution on the cross-section of the MH tank in the 3000th, 5000th, and 7000th seconds, respectively. ***d, e,*** and ***f*** are the temperature distribution on the cross-section of the MH tank in the 3000th, 5000th, and 7000th seconds, respectively.

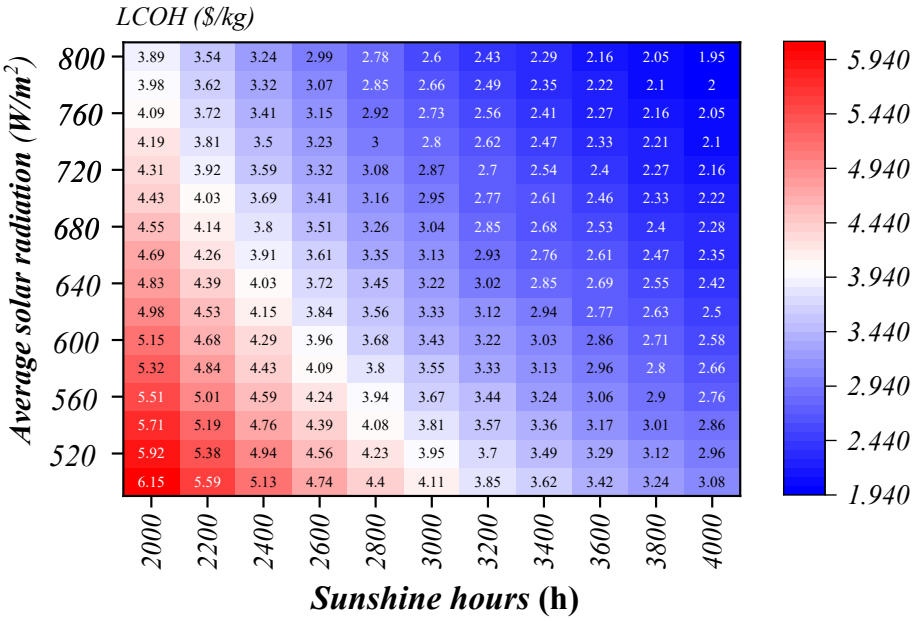

Figure S6. Heat map illustrating the LCOH in production.

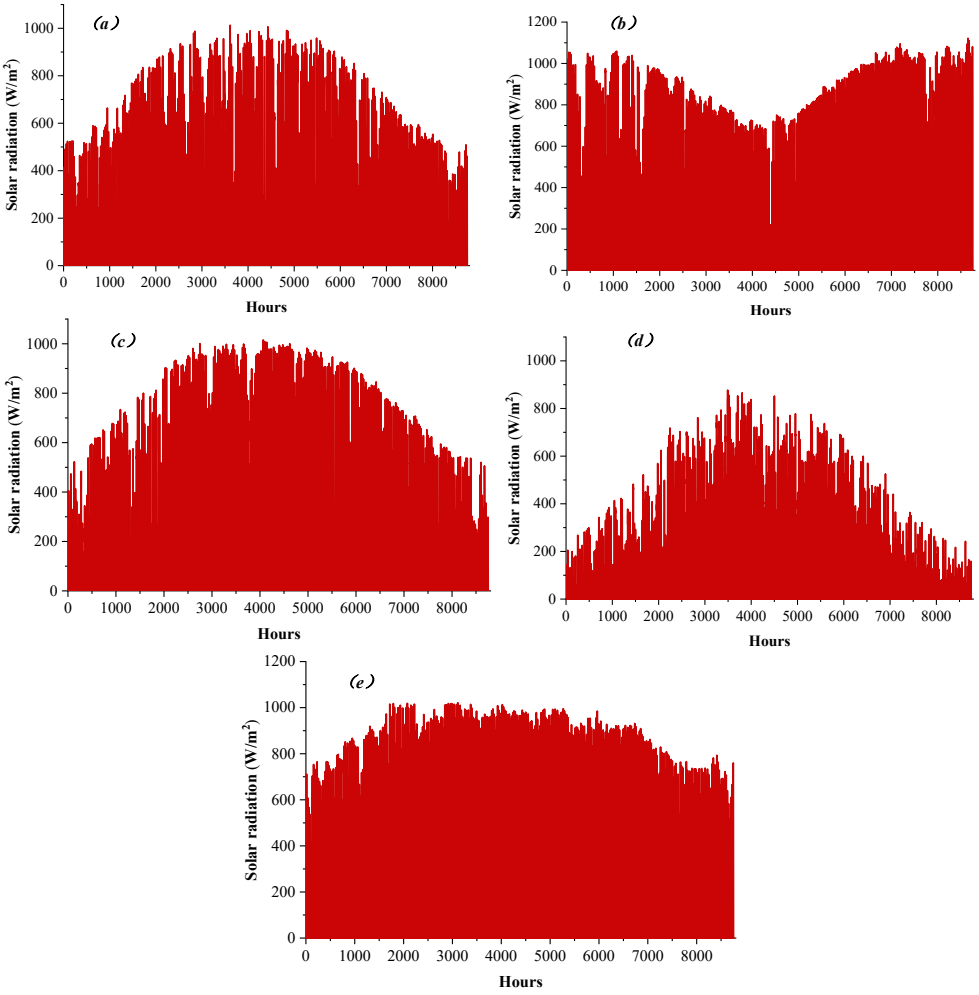

Figure S7. Hourly solar radiation distribution. ***a:*** Jiuquan (China); ***b:*** Queensland (Australia); ***c:*** California (US); ***d:*** Kent (UK); ***e:*** Jeddah (Middle East) [25].

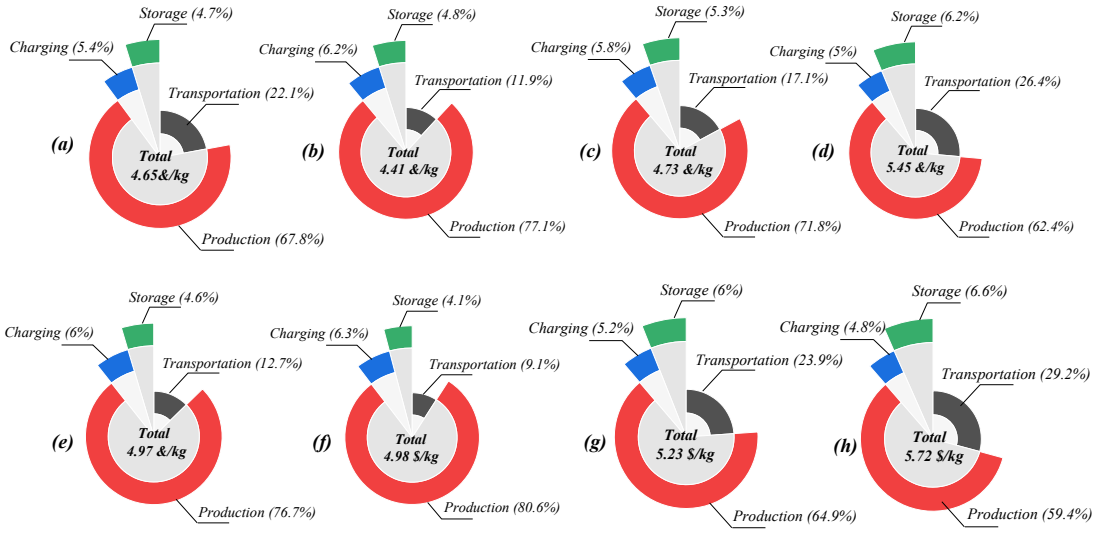

Figure S8. Cost distribution along the optimal magnesium hydrides-based hydrogen transport pathway across various routes. ***a:*** Jiuquan to Urumqi by railway (Ra-A2). ***b:*** Jiuquan to Lanzhou by railway (Ra-B1). ***c:*** Jiuquan to Xi'an by railway (Ra-C1). ***d:*** Jiuquan to Shanghai by railway (Ra-D1). ***e:*** Ordos to Beijing by railway (Ra-E3). ***f:*** Baicheng to Harbin by railway (Ra-F2). ***g:*** Jiuquan to Wuhan by railway (Ra-G1). ***h:*** Jiuquan to Guangzhou by railway (Ra-H).

Table S1. SOEC structure and operating parameters.

Ref	[26]	[27]	[28]	[29]	[30]	[31]	[32]	[33]
Year	2020	2015	2020	2019	2019	2015	2013	2022
Electrolyte	10Sc1CeSZ	YSZ	3YSZ	YSZ	YSZ	YSZ	YSZ	YSZ
Thickness of electrolyte (µm)	160 µm	~10 µm	80 µm	8 µm	8 µm	10 µm	-	8-10 µm
Cathode	NiO/GDC	Ni/8YSZ	Ni/GDC	Ni/YSZ	Ni/YSZ	Ni/YSZ	Ni/YSZ	Ni/YSZ
Cathode flow	18 g/h steam	$H_2 = H_2O$ = 1.11 slm	0.833 SLP (80% H_2O + 9% H_2 + 11%N_2)	22 L/h (90% H_2O + 10% H_2)	90%H_2O-10%H_2	90%H_2O-10%H_2	6 Nl/h H_2, 7.08 Nl/h N_2, and 42 g/h steam	30%CO_2,60%H_2O,10%H_2
Anode	LSCF	LSCF	LSCF/ GDC	LSCF/ CGO	LSCF/ GDC	LSC/CGO	LSCF	LSM-YSZ
Anode flow	1500 Nml/min O2	8.0 slm air	1.0 slpm air	50 L/h O_2	Pure O_2	-	90 Nl/h synthetic air	360 L/hr
Active area (cm^2)	45	80	128	16	16	-	45	-
Current density (A/m^2)	-6000	-5000	-5200	-12500	-12500	-10000	-10000	-15000
Cell temperature (°C)	~780	800	820	800	750	800°	778±6	750
Operation hours	over 30 kh	2.3 kh	3.37 kh	3 kh	1.43 kh	2 kh	9 kh	20 kh
Thermal neutral voltage (V)	1.29	1.284	1.29	-	-	-	-	-
Initial Voltage(V)	1.30	-	-	~1.12	1.385	-	-	-
Degradation rates (%/kh)	0.3-0.4	0.7	0.5	0.59	0.7	0.4	3.8	0.89

Table S2. Parameters of MgH_2-based hydrogen storage materials.

Ref	**[34]**	**[35]**	**[36]**	**[37]**	**[38]**	**[39]**	**[40]**
Year	2017	2021	2022	2021	2024	2015	2017
Materials	MgH_2/5 wt. % $TiMn_2$	10 wt.% nano-Mn modified MgH_2	The MgH_2 system containing 5 wt% Ni90@PHCNSs	60MgH_2@Ti-MX s	MgH_2 + 10 wt% Ti–Mn + 1 wt% CNTs	GR-supported MgH_2 NPs	$Mg_{84.0}Ni_{8.1}Y_{7.9}$
Hydrogenation pressure (Mpa)	0.8	3.2	5	3	3	3	3
Dehydrogenation pressure (Mpa)	0.02	-	static vacuum	0.001	0.00025	0.001	vacuum
Temperature (°C)	250	275	250-300	200	325	200	300
Cycle number	1000	20	50	60	100	100	620
Hydrogen density (wt.%)	5.4	6.4	6.5	4.1	6.4	5.4	~5.2
Capacity retention	>90%	0.92	0.941	95	0.968	0.992	0.83

Table S3. Exergy balance equations for the system components.

Component	Exergy fuel	Exergy product	Exergy destruction
PV array	Ex_{in}	$Ex_{out,use}+Ex_{loss}$	$Ex_{in}- Ex_{out,use}-Ex_{loss}$
SOEC	P_{SOEC}	$Ex_{18}+Ex_{12}-Ex_{11}-Ex_{5}$	$Ex_{5}+Ex_{11}-Ex_{18}-Ex_{12}+P_{SOEC}$
Air compressor	W_c	$Ex_{3}-Ex_{2}$	$Ex_{2}-Ex_{3}+W_c$
HE1	$Ex_{12}-Ex_{13}$	$Ex_{11}-Ex_{10}$	$Ex_{12}+Ex_{10}-Ex_{12}-Ex_{11}$
HE2	$Ex_{20}-Ex_{26}$	$Ex_{4}-Ex_{3}$	$Ex_{20}+Ex_{3}-Ex_{26}-Ex_{4}$
HE3	$Ex_{18}-Ex_{19}$	$Ex_{5}-Ex_{4}$	$Ex_{18}+Ex_{4}-Ex_{19}-Ex_{5}$
HE4	$Ex_{19}-Ex_{20}$	$Ex_{16}-Ex_{15}$	$Ex_{19}+Ex_{15}-Ex_{20}-Ex_{16}$
Pump	W_{pump}	$Ex_{7}-Ex_{6}$	$Ex_{6}-Ex_{7}+W_{pump}$
Condenser	$Ex_{13}-Ex_{14}-Ex_{24}$	$Ex_{8}-Ex_{7}$	$Ex_{13}+Ex_{7}-Ex_{14}-Ex_{24}-Ex_{8}$
Evaporator	$P_{heating}+Ex_{21}-Ex_{22}$	$Ex_{10}-Ex_{9}$	$Ex_{21}+Ex_{9}-Ex_{22}-Ex_{10}+P_{heating}$
Hydrogen compressor	$W_{H2,c}$	$Ex_{17}-Ex_{15}$	$Ex_{15}-Ex_{17}+W_{H2,c}$
Metal hydride bed	Ex_{H2}	$M_{H2}\dot{m}LHV_{H2}+Ex_{21}-Ex_{25}$	$Ex_{H2}-M_{H2}\dot{m}LHV_{H2}-Ex_{21}+Ex_{25}$

Table S4. The compression stage and consumed power corresponding to the hydrogen pressure.

Hydrogen pressure	***N***	$P_{H2,Co}$ [41]
2-8 MPa	1	$P_{H_2,co}=\left(\frac{k}{k-1}\right)\left(\frac{Z}{\eta_{isn}}\right)T_{in}q_mR\left[\left(\frac{P_{out}}{P_{in}}\right)^{\left(\frac{k-1}{k}\right)}-1\right]$
6-25 MPa	2	
17-43 MPa	3	$P_{H_2,co}=N\left(\frac{k}{k-1}\right)\left(\frac{Z}{\eta_{isn}}\right)T_{in}q_mR\left[\left(\frac{P_{out}}{P_{in}}\right)^{\left(\frac{k-1}{Nk}\right)}-1\right]$
35-85 MPa	4	

In **Table S4**, k is the adiabatic exponent of hydrogen; Z is the average compressibility factor; η_{isn} is the isentropic efficiency; T_{in} is the inlet temperature of hydrogen, K; P_{in} and P_{out} is the inlet and outlet pressure of hydrogen, respectively, Pa; q_m is the molar flow rate, mol s^{-1}; N and $P_{H2,co}$ are the compression stages and the consumed power, respectively.

Table S5. The regulations published by Chinese government to produce clean production and utilization of magnesium [42-46].

Year	Department	Name	Strategies
2023.03	**Ministry of Industry and Information Technology of China**	*"Guidelines for the Construction of Intelligent Manufacturing Standard System for Nonferrous Metals Industry" (2023 Edition)*	◆ Promote the digital transformation and intelligent upgrading of the magnesium industry. ◆ By 2025, a basic intelligent manufacturing standards system for the non-ferrous metals industry will be established.
2023.04	**Ministry of Industry and Information Technology of China**	*"Catalogue of Technologies and Products Encouraged for Promotion and Application in the Building Materials Industry" (2023 Edition)*	◆ Magnesium slag has been included in the green cement kiln co-processing technology.
2023.08	**Seven departments, including the Ministry of Industry and Information Technology and the National Development and Reform Commission of China**	*"Work Plan for Stabilizing Growth in the Non-Ferrous Metals Industry"*	◆Carry out regulatory announcements and management of key industries such as copper, aluminum, lead, zinc, and magnesium, and cultivate leading enterprises. ◆Guide the magnesium industry and other enterprises to upgrade processes, improve energy efficiency, and reduce carbon emissions.
2023.12	**National Development and Reform Commission of China**	*"Guidance Catalogue for Industrial Structure Adjustment" (2024 Edition)*	◆Encourage the development of lightweight magnesium alloy materials, new high-efficiency, low-consumption, low-pollution smelting technologies, and comprehensive utilization of smelting waste.
2024.05	**Ministry of Industry and Information Technology of China**	*"Catalogue of recommended technologies and equipment for energy conservation and emission reduction in the national industrial and information technology sector" (2024 edition)*	◆Include magnesium-based solid-state hydrogen storage technology in the recommended catalog for energy-saving and carbon reduction.

Table S6. The capital cost of main components in hydrogen production and storage processes [7,41-51].

Component	Capital cost ($)
Photovoltaic power station	$Z_{PV} = 578 \times P_{PV}$
SOEC system	$Z_{SOEC} = 1192 \times W_{SOEC}$
Air compressor	$Z_{AC} = \frac{75 m_{air}}{0.9 - \eta_{AC}} \frac{P_2}{P_1} \ln\left(\frac{P_2}{P_1}\right)$
Hydrogen compressor	$Z_{HC} = N_{HC} W_{HC} SF$
Heat exchanger	$Z_{HE} = 130 * \left(\frac{A_{HE}}{0.093}\right)^{0.78}$
Pump	$Z_{Pump} = 3500 \left(W_p\right)^{0.41}$
Evaporator	$Z_{EV} = 588 \left(A_{EV}\right)^{0.8}$
Condenser	$Z_{Cond} = 588 \left(A_{Cond}\right)^{0.8}$
Hydrogen charging devices	$Z_{H_2,cha} = N_{H_2,cha} \cdot C_{H_2,cha}$
Hydrogen discharging devices	$Z_{H_2,discha} = N_{H_2,discha} \cdot C_{H_2,discha}$
Hydrogen transportation truck	$Z_{H_2,truck} = N_{H_2,truck} \cdot C_{H_2,truck}$

Table S7. Transportation scenarios and mileage.

Transportation mode	Item	Hydrogen utilization site	Hydrogen production site	Distance
Road+Railway	**Ra-A1**	*Urumqi*	*Kashgar*	1500 km
	Ra-A2	*Urumqi*	*Jiuquan*	1180 km
	Ra-B1	*Lanzhou*	*Jiuquan*	680 km
	Ra-B2	*Lanzhou*	*Yinchuan*	460 km
	Ra-C1	*Xi'an*	*Jiuquan*	1360 km
	Ra-C2	*Xi'an*	*Yinchuan*	800 km
	Ra-C3	*Xi'an*	*Erdos*	760km
	Ra-D1	*Shanghai*	*Jiuquan*	2860 km
	Ra-D2	*Shanghai*	*Yinchuan*	2230 km
	Ra-D3	*Shanghai*	*Erdos*	2050 km
	Ra-D4	*Shanghai*	*Hefei*	630 km
	Ra-E1	*Beijing*	*Jiuquan*	2250 km
	Ra-E2	*Beijing*	*Yinchuan*	1220 km
	Ra-E3	*Beijing*	*Erdos*	930 km
	Ra-E4	*Beijing*	*Baicheng*	1130 km
	Ra-F1	*Harbin*	*Erdos*	2180 km
	Ra-F2	*Harbin*	*Baicheng*	510 km
	Ra-G1	*Wuhan*	*Jiuquan*	2410 km
	Ra-G2	*Wuhan*	*Yinchuan*	1840 km
	Ra-G3	*Wuhan*	*Erdos*	1810 km
	Ra-G4	*Wuhan*	*Hefei*	360 km
	Ra-H1	*Guangzhou*	*Jiuquan*	3410 km
Road	**Ro-A**	*Lanzhou*	*Yinchuan*	430 km
	Ro -B	*Wuhan*	*Hefei*	360 km
	Ro-C	*Shanghai*	*Hefei*	470 km
	Ro-D	*Guangzhou*	*Shaoguan*	220 km
	Ro-E	*Harbin*	*Baicheng*	370 km
Road +River	**Ri-A**	*Shanghai*	*Hefei*	170 km (Road) & 350 km (River)

Nomenclature

A	Area (m^2)
Bg	Flow permeability (m^2)
C	Cost ($)
C_p	Specific heat capacity (kJ kg^{-1} K^{-1})
CRF	Capital recovery factor
d	Thickness/length (m)
D^{eff}	Effective diffusion coefficient
E_{act}	Activation energy (kJ mol^{-1})
E^{OPC}	Open circuit potential (V)
Ex	Exergy value (kJ)
F	Faraday's constant (C mol^{-1})
G	Solar irradiance (W m^{-2})
h	Specific enthalpy (kJ)
H/M	Metal ratio per metal atom
i	Interest rate (%)
J	Current density (A m^{-2})
L	thickness of the electrolyte (m)
LHV	lower heat value (kJ kg^{-1})
M	Molar weight (g mol^{-1})
MH	Metal hydride
μ	Dynamic viscosity (Pa s)
μ_p	Power thermal coefficient (% $°C^{-1}$)
ξ	Electrode tortuosity
π	Pressure ratio
ρ	Density (kg m^{-3})
λ	Thermal conductivity (W m^{-1} K^{-1})
τ	Operating hours (h)

Subscripts and Superscripts

act	Activation overpotential
CAP	Capital expenditure
cell	Electrolytic cells
cha	Charging
con	Concentration overpotential
Cond	Condenser
consumed	Consumed heat
cool	Cool fluid
D	Exergy destruction
de	Dehydrogenation
discha	Discharging
ele	Electrolysis process

N	Number
n	Electrode porosity
n_e	Amounts of electrons
$NOCT$	Nominal operating cell temperature (K)
P	Power (kW)/Pressure (Pa)
Q	Heat (kJ)
q	Heat flux (W m^{-2})
R	Universal gas constant (J kg^{-1} K^{-1})
T	Temperature (K)
U_f	Steam utilization factor
y_i	Molar fraction of the species
Z	Average compressibility factor/ Cost ($)
Greek symbols	
γ	Pre-exponential factor (A m^{-2})
ΔH	Reacted enthalpy (kJ mol^{-1})
η	Efficiency/ overpotential (V)
ε	Effectiveness of heat exchanger/Chemical energy factor
ϕ	Resistance of the electrolyte Maintenance factor
λ	Thermal conductivity (W m^{-1} K^{-1})
κ	Adiabatic exponent

ele,de	Dehydrogenation consumed electricity
ele,co	Compression consumed electricity
eq	Equilibrium
env	Environment
Eva	Evaporator
gas	Gas
HE	Heat exchanger
heat	Heat fluid
i	Electrode
in	Inlet
loss	Exergy loss
ohm	Ohmic overpotential
out	Outlet
O&M	Operation and management
Pro	Production
PV	Photovoltaic
ref	Reference
Steam	Steam
S&T	Storage and transportation
Train	Train

Reference

1 Hammou T. Off grid PV system for hydrogen production using PEM methanol electrolysis and an optimal management strategy. *Int J Hydrogen Energy*, 2017, 42(30): 19432-19445.

2 Ceylan C, Devrim Y. Design and simulation of the PV/PEM fuel cell based hybrid energy system using MATLAB/Simulink for greenhouse application. *Int J Hydrogen Energy*, 2021, 46(42): 22092-22106.

3 Menon V, Vinod M. J, Olaf D. A mathematical model to analyze solid oxide electrolyzer cells (SOECs) for hydrogen production. *Chem Eng Sci*, 2014, 110: 83-93.

4 Wang T, Guo S, Li X, et al. A meta-network-based risk evaluation and control method for industrialized building construction projects. *J Clean Prod*, 2018, 205: 552-564.

5 Chen X, Liu Q, Xu J, et al. Thermodynamic study of a hybrid PEMFC-solar energy multi-generation system combined with SOEC and dual Rankine cycle. *Energ Convers Manage*, 2020, 226: 113512.

6 Karittha I-O, Nuttawut V, Dang S, et al. Flowsheet-based model and exergy analysis of solid oxide electrolysis cells for clean hydrogen production. *J Clean Prod*, 2018,170: 1-13.

7 Cao Y, Towhid P. A solar-driven lumped SOFC/SOEC system for electricity and hydrogen production: 3E analyses and a comparison of different multi-objective optimization algorithms. *J Clean Prod*, 2020, 271: 122457.

8 Ni M, Michael K H L. Dennis Y.C. L. A modeling study on concentration overpotentials of a reversible solid oxide fuel cell. *J Power Sources*, 2006, 163(1): 460-466.

9 Li Q, Lu Y, Luo Q, et al. Thermodynamics and kinetics of hydriding and dehydriding reactions in Mg-based hydrogen storage materials. *J Magnes Alloy*, 2021, 9(6): 1922-1941.

10 Xin F-T, Kim M, Yasuda K, et al. Strategies to enhance hydrogen storage performances in bulk Mg-based hydrides. *J Mater Sci Technol*, 2023, 153: 139-158.

11 Mellouli S, Dhaou H, Askri F, et al. Hydrogen storage in metal hydride tanks equipped with metal foam heat exchanger. *Int J Hydrogen Energy*, 2009, 34(23): 9393-9401.

12 Chaise A, Rango P.d, Marty P, et al. Experimental and numerical study of a magnesium hydride tank. *Int J Hydrogen Energy*, 2010, 35(12): 6311-6322.

13 Cengel YA. Heat and mass transfer, a practical approach[M]. McGraw-Hill; 2007.

14 Wang X, Yang C, Huang M, et al. Off-design performances of gas turbine-based CCHP combined with solar and compressed air energy storage with organic Rankine cycle. *Energy Convers Manag*, 2018, 156:626-638.

15 Wang S, Chen G, Fang M, et al. A new compressed air energy storage refrigeration system. *Energy Convers Manag*, 2006, 47(18-19): 3408-3416.

16 Wang X, Yang C, Huang M, et al. Multi-objective optimization of a gas turbine-based CCHP combined with solar and compressed air energy storage system.

Energy Convers Manag, 2018, 164: 93-101.

17 Agbaje M A, Akkaya A V. Electrochemical-energy- exergy analysis of reversible solid oxide cell-based small-scale stand-alone energy storage system. *Case Stud Therm Eng*, 2023, 52: 103732.

18 Ahmadi P, Dincer I, Marc A. R. Exergy, exergoeconomic and environmental analyses and evolutionary algorithm based multi-objective optimization of combined cycle power plants. *Energy*, 2011, 36(10): 5886-5898.

19 Ozden E, Tari I. Energy–exergy and economic analyses of a hybrid solar–hydrogen renewable energy system in Ankara, Turkey. *Appl Therm Eng*, 2016, 99: 169-178.

20 Kubilay B, Mustafa N. Energy, exergy, sustainability evaluation of the usage of pyrolytic oil and conventional fuels in diesel engines. *Process Safe Environ*, 2024, 181: 324-333.

21 Wang J, Al-attab K A, Heng T Y. Techno-economic and thermodynamic analysis of solid oxide fuel cell combined heat and power integrated with biomass gasification and solar assisted carbon capture and energy utilization system. *Energy Convers Manag*, 2023, 280: 116762.

22 Alirahmi S M, Razmi A R, Arabkoohsar A. Comprehensive assessment and multi-objective optimization of a green concept based on a combination of hydrogen and compressed air energy storage (CAES) systems. *Renew Sust Energy Rev*, 2021, 142: 110850.

23 Lucas T R, Ferreira A F, Pereira R.B.S, et al. Hydrogen production from the

Wind Float Atlantic offshore wind farm: A techno-economic analysis. *Appl Energy*, 2022, 310: 118481.

24 Ebbesen S D, Graves C, Mogensen M. Production of Synthetic Fuels by Co-Electrolysis of Steam and Carbon Dioxide. *Int J Green Energy*, 2009, 6(6): 646-660.

25 Shao L, Lin X, Bian L, et al. Engineering control strategy of hydrogen gas direct-heating type Mg-based solid state hydrogen storage tanks: A simulation investigation. *Appl Energy*, 2024,275, 124134.

26 The data was obtained from the POWER Project's Hourly 2.3.6 version on 01/01/2023-31/12/2023.

27 Josef S, Hendrik P, Annabelle B. Solid Oxide Electrolyser Cell Testing Up to the Above 30,000 h Time Range. *ECS Transactions*, 2020, 97(7): 553.

28 Fang Q, Blum L, Menzler N H, et al. Performance and Degradation of Solid Oxide Electrolysis Cells in Stack. *J Electrochem Soc*, 2015, 162: F907.

29 Lang M, Raab S, Lemcke M.S et al. Long-Term Behavior of a Solid Oxide Electrolyzer (SOEC) Stack. *FUEL CELLS*, 2020, 20(6): 690–700.

30 Ovtar S, Tong X, Bentzen J J, et al. Boosting the performance and durability of Ni/YSZ cathode for hydrogen production at high current densities via decoration with nano-sized electrocatalysts. *Nanoscale*, 2019, 11, 4394-4406.

31 Tong X, Hendriksen P V, Hauch A, et al. Development of Solid Oxide Electrolysis Cells for Hydrogen Production at High Current Densities. *ECS Trans*, 2019, 91: 2433.

32 Hauch.A, Brodersen.K, Chen.M,et al.Ni/YSZ electrodes structures optimized for increased electrolysis performance and durability. *Solid State Ionic*s,2016,293:27-36.

33 Tietz F, Sebold D, Brisse A, et al. Degradation phenomena in a solid oxide electrolysis cell after 9000 h of operation. *J Power Sources*, 2013, 223: 129-135.

34 Kamkeng A D N, Wang M. Long-term performance prediction of solid oxide electrolysis cell (SOEC) for CO_2/H_2O co-electrolysis considering structural degradation through modelling and simulation. *Chem Eng J*, 2022, 429: 132158.

35 El-Eskandarany, M.S., Shaban, E., Aldakheel, F. et al. Synthetic nanocomposite MgH_2/5 wt. % $TiMn_2$ powders for solid-hydrogen storage tank integrated with PEM fuel cell. *Sci Rep*, 2017, 7: 13296.

36 Chen Y, Zhang H, Wu F, et al. Mn nanoparticles enhanced dehydrogenation and hydrogenation kinetics of MgH_2 for hydrogen storage. *Transactions of Nonferrous Metals Society of China*, 2021, 31(11), 3469-3477.

37 Wang S, Gao M, Yao Z, et al. High-loading, ultrafine Ni nanoparticles dispersed on porous hollow carbon nanospheres for fast (de)hydrogenation kinetics of MgH_2. *J Magnes Alloy*, 2022, 10(12): 3354-3366.

38 Zhu W, Ren L, Lu C, et al. Nanoconfined and in Situ Catalyzed MgH_2 Self-Assembled on 3D Ti_3C_2 MXene Folded Nanosheets with Enhanced Hydrogen Sorption Performances. *ACS Nano*, 2021, 15, 11, 18494–18504.

39 Lu Z, Liu H, Luo H, et al. Effect of $Ti_{0.9}Zr_{0.1}Mn_{1.5}V_{0.3}$ alloy catalyst on hydrogen storage kinetics and cycling stability of magnesium hydride. *Chem Eng J*, 2024,

479: 147893.

40 Xia G, Tan Y, Chen X, et al. Monodisperse Magnesium Hydride Nanoparticles Uniformly Self-Assembled on Graphene. *Adv Mater*, 2015, 27(39): 5981-5988.

41 Li Q, Li Y, Liu B, et al. The cycling stability of the in situ formed Mg-based nanocomposite catalyzed by YH_2. *J Mater Chem. A*, 2017, 5, 17532-17543.

42 Mohd A K, Cameron Y, Catherine M, et al. The Techno-Economics of Hydrogen Compression.2021. https://transitionaccelerator.ca/wp-content/uploads/2023/04/TA-Technical-Brief-1.1_TEEA-Hydrogen-Compression_PUBLISHED.pdf.

43 Ministry of Industry and Information Technology of China, Guidelines for the Construction of Intelligent Manufacturing Standard System for Nonferrous Metals Industry (2023 Edition) 2023.https://www.miit.gov.cn/zwgk/zcwj/wjfb/tz/art/2023/art_328702b2e33443f5bfc4ff8b4f9d4032.html.

44 Ministry of Industry and Information Technology of China, Catalogue of Technologies and Products Encouraged for Promotion and Application in the Building Materials Industry (2023 Edition), 2023. https://www.gov.cn/zhengce/zhengceku/2023-04/26/content_5753232.htm.

45 Ministry of Industry and Information Technology of China, Work Plan for Stabilizing Growth in the Non-Ferrous Metals Industry, 2023. https://www.gov.cn/gongbao/2023/issue_10806/202311/content_6913831.html.

46 National Development and Reform Commission of China, Guidance Catalogue

for Industrial Structure Adjustment, (2024 Edition), 2024. https://www.gov.cn/zhengce/202401/content_6924187.htm.

47 Ministry of Industry and Information Technology of China, Catalogue of recommended technologies and equipment for energy conservation and emission reduction in the national industrial and information technology sector, (2024 edition), 2024. https://www.miit.gov.cn/zwgk/wjgs/art/2024/art_3e24359927ff4e929b2b92808d1c3a37.html.

48 Wang J, Al-attab K A, Heng T Y. Techno-economic and thermodynamic analysis of solid oxide fuel cell combined heat and power integrated with biomass gasification and solar assisted carbon capture and energy utilization system. *Energy Convers Manag*, 2023, 280: 116762.

49 Alirahmi S M, Razmi A R, Arabkoohsar A. Comprehensive assessment and multi-objective optimization of a green concept based on a combination of hydrogen and compressed air energy storage (CAES) systems. *Renew Sust Energy Rev*, 2021, 142: 110850.

50 Brian D. James. HTE Stack Manufacturing Cost Analysis. 2022. https://www.energy.gov/sites/default/files/2022-03/HTE%20Workshop-Strategic%20Analysis.pdf.

51 Huang Z.F, Chen W.D, Wan Y.D, et al. Techno-economic comparison of different energy storage configurations for renewable energy combined cooling heating and power system. *Appl Energy*, 2024, 356: 122340.

52 Ghaebi H, Farhang B, Parikhani T, et al. Energy, exergy and exergoeconomic analysis of a cogeneration system for power and hydrogen production purpose based on TRR method and using low grade geothermal source. *Geothermics*, 2018, 71: 132-145.